BULLETIN OF THE POLISH ACADEMY OF SCIENCES
TECHNICAL SCIENCES, Vol. 74(3), 2026, Article number: e158301
DOI: 10.24425/bpasts.2026.158301

Active disturbance rejection control for rate-controlled input underactuated systems: Application to a reaction wheel pendulum

Jacek MICHALSKI*, Mikołaj MROTEK, Stefan BROCK, Marek RETINGER, and Piotr KOZIERSKI

Faculty of Control, Robotics and Electrical Engineering, Institute of Robotics and Machine Intelligence, Poznan University of Technology, Piotrowo 3a, 60-965 Poznan, Poland

Abstract. The paper deals with the application of Active Disturbance Rejection Control (ADRC) to underactuated systems with rate-controlled input dynamics, illustrated by a reaction wheel pendulum (RWP). In this class of plants, the derivative of the control signal appears in the input–output dynamics, which violates the standard integrator-chain assumption underlying classical ADRC and may degrade observer performance and closed-loop quality. To overcome this difficulty, two ADRC modifications that exploit partial model information are proposed. First, a reduced-order input–output model is derived, in which the derivative behavior of the input is analytically compensated, resulting in an affine input form compatible with the conventional ADRC structure. Second, a dual-output ADRC scheme is developed, combining an extended state observer with an inner-loop LQR-based state feedback, which enables simultaneous stabilization of the pendulum angle and the wheel speed despite a single actuator. For both variants, Lyapunov-based stability conditions are obtained. The proposed controllers are implemented and experimentally verified on a real reaction wheel pendulum setup. Swing-up-and-balance experiments around the lower and upper equilibrium positions show that the modified ADRC schemes reduce overshoot and oscillations, mitigate steady-state drift, and improve control performance with respect to a baseline model-free ADRC.

Keywords: active disturbance rejection control; extended state observer; reaction wheel pendulum; underactuated systems; rate-controlled input.

1. INTRODUCTION

Robust control methods capable of coping with model uncertainties and external disturbances have been a central topic in control theory and practice for decades. In this context, the concept of active disturbance rejection control (ADRC), originally proposed by Han and further developed by Gao and many other authors, has attracted substantial attention [1, 2]. ADRC combines the structural simplicity of classical PID—relying on the regulation error and a small number of tuning parameters—with the use of an extended state observer (ESO) that estimates both the plant states and the so-called total disturbance, which aggregates model uncertainties and external perturbations [3, 4]. As a result, it enables the design of feedback controllers that require only limited model information, which makes ADRC particularly attractive for industrial applications and for complex mechatronic systems.

Over the past two decades, numerous works have systematized ADRC methodology and its theoretical underpinnings, including both state-space and transfer-function formulations, as well as discrete-time implementations [3–7]. Alongside the original model-free formulation based on an integrator-chain approximation with known input gain, various model-based variants (such as generalized ADRC, GADRC) have been proposed, in which a known part of the linear model is explicitly incorporated in the controller design [8–10]. An important line of research concerns ESO tuning and adaptation of ADRC parameters, in particular in the presence of measurement noise and stochastic disturbances, as well as in applications to high-order and torsional systems [11–18]. These developments facilitate a more systematic comparison between ADRC and classical control methods and support its practical deployment.

ADRC has been successfully applied in a wide range of domains, including power systems and power electronics [13, 19], electric drives and torsional systems [14, 15], as well as robotics and mechatronics [20]. In robotic and motion-control applications, ADRC has been investigated for nonlinear and underactuated systems, such as inverted pendulums, Furuta pendulums, and other benchmark setups used to study advanced control strategies [20–22]. A representative example of a nonlinear underactuated plant is the reaction wheel pendulum (RWP), widely used as a laboratory benchmark for systems with a limited number of actuators [21, 23–25]. The RWP features two nonlinearly coupled subsystems, the pendulum arm and the reaction wheel, while the control input acts only through the wheel torque. A detailed formulation of the RWP dynamics was previously

*e-mail: jacek.michalski@put.poznan.pl

Manuscript submitted 2025-12-10, revised 2026-01-22, initially accepted for publication 2026-02-23, published in May 2026.

presented in [26], where the analysis focused on the standard full state-feedback configuration, in contrast to the ADRC architecture considered in this work.

From the viewpoint of ADRC synthesis, an important difficulty is that, in the linearized model of the RWP around the upright position, the control input typically enters in the form of its derivative, leading to a rate-controlled input structure. In contrast, standard ADRC formulations assume that the plant can be transformed into an integrator-chain canonical form, where the control signal appears directly in the equation of the highest derivative of the output [1, 3]. A direct application of conventional ADRC to plants with differentiating-type input dynamics may therefore lead to problems with ESO bandwidth selection, increased sensitivity to measurement noise, and degradation of closed-loop performance [4, 5]. At the same time, most existing works on RWP focus on nonlinear control strategies (including energy-based and differential-flatness-based approaches) that are not easily translated into a simple, practitioner-oriented ADRC design procedure [21, 23, 24]. As a consequence, the systematic adaptation of ADRC to underactuated plants with derivative-input dynamics remains relatively less explored.

Nonlinear control of reaction-wheel pendulums and related underactuated systems has been extensively studied in the literature. Early works include hybrid swing-up and balancing strategies [21] and the comprehensive monograph on modeling and nonlinear control of the RWP [27]. More recent contributions propose Lyapunov-based nonlinear controllers and inverse optimal formulations for global stabilization in continuous and discrete time [28, 29], as well as intelligent and fuzzy-logic-based schemes for dual-axis RWPs and similar benchmarks [30]. Reaction-wheel-based stabilization has also been investigated in other platforms, such as self-balancing bicycles [31] and reaction-wheel pendula used as attitude-control demonstrators in aerospace-oriented studies [32]. These methods exploit detailed nonlinear models and are tailored to specific tasks (global stabilization, trajectory tracking, or optimality), whereas the present work aims at adapting the classical ADRC paradigm to systems with rate-controlled input and underactuation. For this reason, the baseline model-free ADRC serves as the main reference point in comparison to presented in the paper, and the emphasis is placed on how limited model information can be incorporated to improve ADRC performance. Unlike nonlinear RWP control designs aimed at global stabilization or optimal performance, the present work focuses on assessing the behavior of basic ADRC structures in the presence of derivative-input dynamics.

The present paper continues the authors' previous research on the impact of model structure and observer tuning on ADRC algorithms, conducted both in deterministic and stochastic settings and for various classes of mechanical systems [33–36]. To the best of the authors' knowledge, the novelty of this work lies in adapting ADRC to systems with derivative input dynamics, demonstrated experimentally on a reaction wheel pendulum. Two ADRC modifications are proposed: (i) an order-reduction approach that compensates the rate-controlled input behavior, and (ii) a dual-output ADRC structure with an inner-loop LQR-based state feedback.

The main contributions of the paper can be summarized as follows:

- formulation of an ADRC-compatible reduced-order input-output model for derivative-input systems, allowing one to recover an effective integrator-chain structure;
- development of a two-output ADRC scheme with an LQR-based inner loop, ensuring simultaneous stabilization of both the pendulum angle and the wheel speed;
- unified Lyapunov-based stability proofs for the proposed ADRC variants and their experimental validation on a real underactuated RWP setup.

The remainder of the paper is organized as follows. Section 2 introduces the considered laboratory setup, the mathematical model of the reaction wheel pendulum, and the resulting input-output representation with rate-controlled input. Section 3 briefly recalls the fundamentals of ADRC synthesis and presents in detail the two proposed modifications: the reduced-order approach and the dual-output ADRC with an embedded LQR loop. Section 4 reports experimental results obtained on the real RWP system, including a comparison with a reference ADRC design and an analysis of the influence of key design parameters on the closed-loop performance. Finally, Section 5 concludes the paper and outlines directions for future research, in particular the extension of the proposed methods to other classes of underactuated, rate-controlled input systems.

2. RWP SYSTEM DESCRIPTION

2.1. Mathematical model

The scheme of the RWP system considered in this paper, with the most important variables highlighted, is shown in Fig. 1. The input is the voltage signal u and three signals can be considered as the controlled variables: motor shaft position θ, velocity ω, and the pendulum arm position φ.

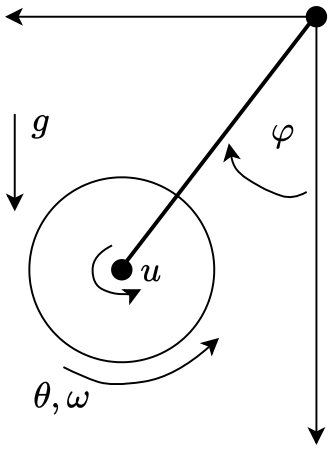

Fig. 1. Diagram of the considered plant

The nonlinear equations of motion of the RWP system, based on [26], are given as follows:

$$\begin{cases} J_\varphi \ddot{\varphi} = -m_p g l \sin(\varphi) - \dfrac{k_t}{R}(u - k_t\omega) + \mu_\theta \omega - \mu_\varphi \dot{\varphi}, \\ J_\theta \dot{\omega} = \dfrac{k_t}{R}(u - k_t\omega) - \mu_\theta \omega, \\ \dot{\theta} = \omega, \end{cases} \tag{1}$$

where J_φ and J_θ denote the moments of inertia of the pendulum arm and the actuator, respectively, m_p is the mass of the pendulum, g is the gravitational constant, l is the length between center of mass and rotational axis, μ_φ and μ_θ are damping coefficients in the arm and motor shaft axes, k_t and R are the drive parameters: electromagnetic constant and resistance[1].

The set of equations (1) can be rewritten in a more compact form for the controller synthesis purposes:

$$\begin{cases} \ddot{\varphi} = -a_0 \sin(\varphi) - a_1 \dot{\varphi} + c_1 \omega - b_0 u, \\ \dot{\omega} = -\gamma_J (c_1 \omega - b_0 u), \end{cases} \tag{2}$$

where

$$a_0 = \frac{m_p g l}{J_\varphi}, \quad a_1 = \frac{\mu_\varphi}{J_\varphi}, \quad c_1 = \frac{k_t^2 + \mu_\theta R}{J_\varphi R},$$

$$b_0 = \frac{k_t}{J_\varphi R}, \quad \gamma_J = \frac{J_\varphi}{J_\theta}.$$

The motor shaft position θ is not used directly in the control process, so the last equation from (1) can be omitted here.

The torque balance for the rotor is written in the frame attached to the arm, so the inertial effects associated with the arm motion appear in (2) and do not produce an explicit $\ddot{\varphi}$ term, in accordance with [26].

The general input-output form of the model (2) can be derived by differentiating the first equation of (2) and substituting ω and $\dot{\omega}$ from the second one

$$\varphi^{(3)} = -a_0 c_1 \gamma_J \sin(\varphi) - (a_0 \cos(\varphi) + a_1 c_1 \gamma_J)\dot{\varphi} + \\ - (a_1 + c_1 \gamma_J)\ddot{\varphi} - b_0 \dot{u}. \tag{3}$$

To obtain the input-output relation, the first equation of (2) is differentiated with respect to time and the variables ω and $\dot{\omega}$ are explicitly expressed in terms of φ, $\dot{\varphi}$, $\ddot{\varphi}$, u and $\dot{u}$. This leads to the equivalent representation

$$\begin{cases} \varphi^{(3)} = -a_0 \cos(\varphi)\dot{\varphi} - a_1 \ddot{\varphi} + c_1 \dot{\omega} - b_0 \dot{u}, \\ \dot{\omega} = -\dfrac{J_\varphi}{J_\theta}(c_1 \omega - b_0 u), \\ \omega = \dfrac{1}{c_1}(\ddot{\varphi} + a_0 \sin(\varphi) + a_1 \dot{\varphi} + b_0 u), \end{cases} \tag{4}$$

from which the input-output dynamics follow after substituting $\dot{\omega}$ and ω into the first equation. Here, $\varphi^{(3)} = \dfrac{d^3\varphi}{dt^3}$.

For the control purposes, one can obtain the linear approximation of the RWP system model. After Taylor linearization at the equilibrium point $\varphi_0 = k\pi$ ($k \in \mathbb{N}$), $\dot{\varphi} = 0$, and $\ddot{\varphi} = 0$, the linear input-output model is obtained:

$$\varphi^{(3)} = -a_0 c_1 \gamma_J \cos(\varphi_0)\varphi - (a_0 \cos(\varphi_0) + a_1 c_1 \gamma_J)\dot{\varphi} + \\ - (a_1 + c_1 \gamma_J)\ddot{\varphi} - b_0 \dot{u}. \tag{5}$$

Note that in the input-output dependency (5) the derivative character of input signal can be seen, which is a challenge in the ADRC synthesis.

Here $\varphi_0 = k\pi$ ($k \in \mathbb{Z}$) denotes either the lower equilibrium (k even) or the upper equilibrium (k odd). After angle normalization both equilibria satisfy $\varphi = 0$, so the linearization does not include a constant offset term.

Angle normalization

In the experimental setup the pendulum angle φ evolves on the full circle and both equilibrium points (the lower and the inverted one) must be stabilized. For control purposes it is therefore convenient to normalize the angular position to local coordinates associated with the corresponding equilibrium points. The normalized angles for the upper and lower positions are defined as follows, where the subscripts up and down refer to the upper (inverted) and lower equilibria, respectively:

$$\begin{cases} \varphi_{\text{up}} = \operatorname{atan2}(\sin(\varphi + \pi), \cos(\varphi + \pi)), \\ \varphi_{\text{down}} = \operatorname{atan2}(\sin\varphi, \cos\varphi), \end{cases} \tag{6}$$

where atan2$(\cdot)$ denotes the two-argument arctangent, ensuring continuity on the entire $[-\pi, \pi)$ range. As a result, both equilibrium points are mapped to the common reference value $y_r = 0$, which allows one to use the same ADRC structure and tuning procedure for both stabilization tasks without loss of generality.

2.2. General description of the laboratory stand

The research was carried out using the Inteco reaction wheel pendulum [25], which is an inverted pendulum-type device. It is equipped with a DC (direct current) motor to move the reaction wheel. The motor is controlled by a PWM (pulse width modulation) signal through the power interface integrated with the dedicated board, connected to the workstation. For precise position measurement, two encoders are used. The flywheel angle encoder has a resolution of 1024 impulses per revolution and the pendulum axis encoder has a resolution of 5000 imp/rev. The construction is also equipped with additional counterweights that allow adjusting the dynamic characteristics of the unit. The most important advantages of the platform are its fully integrated software with the MATLAB/Simulink environment and the unlimited rotation of the arm. A photo of the laboratory setup used in the experiments is presented in Fig. 2.

[1]The dynamics of the motor current were omitted in the considerations.

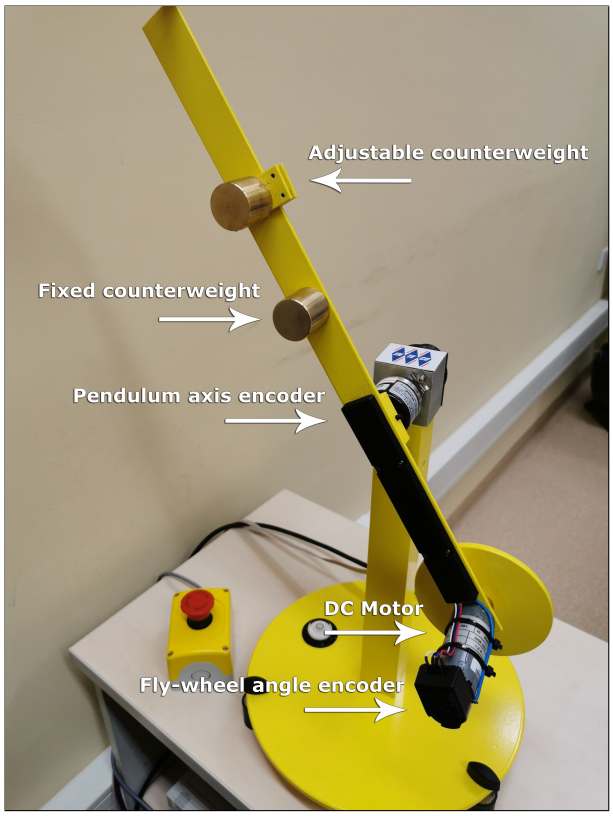

Fig. 2. The laboratory setup used during the experiments – Inteco Reaction Wheel Pendulum. The most important parts were highlighted

3. ADRC CONTROL APPROACHES

3.1. Preliminaries

In the ADRC control system, it is assumed that the control plant is transformed into an integrator-chain form [2]. The system model is given by the equation

$$y^{(n)} = f\left(y, \dot{y}, ..., y^{(n-1)}, u, d\right) + \hat{b}_0 u, \tag{7}$$

where y is the system output, $y^{(n)} = \frac{d^n y}{dt^n}$ is the n-th output signal derivative, $f(\cdot)$ is the total disturbance function, d is the external disturbance signal, u is the input signal, and $\hat{b}_0$ is the estimated scaling factor in the input path.

Total disturbance function is defined as follows [37]

$$f(\cdot) = g(\cdot) + d + (b_0 - \hat{b}_0)u, \tag{8}$$

where function $g(\cdot)$ represents the unmodeled parts of the system. In the remainder of this paper, we assume that the true input gain b_0 is known (as well as its sign); hence $|b_0 - \hat{b}_0| = 0$.

The system (7) can be described using state-space representation

$$\begin{cases} \dot{\underline{x}} = \mathbf{A}\underline{x} + \underline{b}\hat{b}_0 u + \underline{h}\dot{f}, \\ y = \underline{c}^{\top}\underline{x}, \end{cases} \tag{9}$$

for the extended state vector in the form

$$\underline{x} = \begin{bmatrix} x_1 & x_2 & \dots & x_n & x_{n+1} \end{bmatrix}^{\top} = \begin{bmatrix} y & \dot{y} & \dots & y^{(n-1)} & f(\cdot) \end{bmatrix}^{\top}$$

and matrices:

$$\mathbf{A} = \begin{bmatrix} 0 & 1 & 0 & \cdots & 0 & 0 \\ 0 & 0 & 1 & \cdots & 0 & 0 \\ \vdots & \vdots & \vdots & \ddots & \vdots & \vdots \\ 0 & 0 & 0 & \cdots & 1 & 0 \\ 0 & 0 & 0 & \cdots & 0 & 1 \\ 0 & 0 & 0 & \cdots & 0 & 0 \end{bmatrix} \in \mathbb{R}^{(n+1)\times(n+1)},$$

$$\underline{b} = \begin{bmatrix} 0 \\ 0 \\ \vdots \\ 0 \\ 1 \\ 0 \end{bmatrix} \in \mathbb{R}^{n+1}, \quad \underline{h} = \begin{bmatrix} 0 \\ 0 \\ \vdots \\ 0 \\ 0 \\ 1 \end{bmatrix} \in \mathbb{R}^{n+1}, \quad \underline{c} = \begin{bmatrix} 0 \\ 0 \\ \vdots \\ 0 \\ 0 \\ 0 \end{bmatrix} \in \mathbb{R}^{n+1}. \tag{10}$$

Extended state observer

In the ADRC framework, the extended state observer reconstructs the system state from the available input-output signals and provides an online estimate of the total disturbance, including unmodeled dynamics and external perturbations. This estimate is then compensated in the control law to achieve disturbance rejection.

For the considered system structure, the ESO is given as follows [8]:

$$\begin{cases} \dot{\hat{\underline{x}}} = \left(\mathbf{A} - \underline{l}\underline{c}^{\top}\right)\hat{\underline{x}} + \underline{b}\hat{b}_0 u + \underline{l}y, \\ \hat{y} = \underline{c}^{\top}\hat{\underline{x}}, \end{cases} \tag{11}$$

where $\hat{\underline{x}} = \begin{bmatrix} \hat{x}_1 & \hat{x}_2 & \dots & \hat{x}_{n+1} \end{bmatrix}^{\top} = \begin{bmatrix} \hat{y} & \hat{\dot{y}} & \dots & \hat{f} \end{bmatrix}^{\top}$ is the estimated state vector, $\underline{l} = \begin{bmatrix} l_1 & l_2 & \dots & l_{n+1} \end{bmatrix}^{\top}$ is the vector of the ESO gains.

The most popular method of parameterizing the ESO, used in practice, is the pole placement approach [8]. It was assumed that the poles are placed at a single multiple eigenvalue $s = -\omega_o$:

$$\det\left(s\mathbf{I} - (A - \underline{l}\underline{c}^{\top})\right) = (s + \omega_o)^{n+1}, \tag{12}$$

where ω_o is the observer bandwidth value, $\mathbf{I}$ is the identity matrix.

Controller

The main purpose of the outer control loop in the ADRC scheme is to obtain the behavior of the integral chain by introducing a new input signal

$$y^{(n)} = u_0. \tag{13}$$

In this loop, the simple state feedback can be applied

$$u_0 = k_1 y_r - \underline{k}^{\top}\hat{\underline{x}}_n, \tag{14}$$

where y_r is the reference value, $\underline{k} = \begin{bmatrix} k_1 & \dots & k_n \end{bmatrix}^{\top}$ is the feedback gains vector, and $\hat{\underline{x}}_n = \begin{bmatrix} \hat{x}_1 & \dots & \hat{x}_n \end{bmatrix}^{\top}$ is the state vector

without the disturbance function. The component $k_1 y_r$ is responsible for unit static gain of the control system.

Comparing (13) with model (7), under the assumptions $|b_0 - \hat{b}_0| < \epsilon$ and $|\hat{x}_{n+1} - f| \to 0$, the final control law can be obtained

$$u = \frac{1}{\hat{b}_0}(u_0 - \hat{x}_{n+1}). \tag{15}$$

Similarly to the ESO gain selection, pole placement can be used to compute the elements of $\underline{k}$.

It was assumed that the poles are placed at a single multiple eigenvalue $s = -\omega_c$:

$$\det\left(s\mathbf{I} - (\mathbf{A}_n - \underline{b}_n \underline{k}^{\mathrm{T}})\right) = (s + \omega_c)^n, \tag{16}$$

where ω_c is the desired closed-loop system bandwidth, $\mathbf{A}_n$ and $\underline{b}_n$ are the matrices with n first rows and columns of $\mathbf{A}$ and $\underline{b}$ (10), respectively.

Remark 1. Model (5) cannot be directly fitted to the ADRC structure, due to the presence of the input derivative term $\dot{u}$. Assuming the derivative in the input path in the state-space model, i.e., $\underline{c}^{\top} = \begin{bmatrix} 0 & 1 & 0 & \dots & 0 \end{bmatrix}$, the pair $(\mathbf{A}, \underline{c})$ (10) becomes unobservable.

The possible approach to solve this problem could be velocity control, which requires increasing the order of the algorithm (integrating the determined control signal). However, in this work, the basic ADRC is assumed, omitting information about the derivative in the input path.

For systems with underactuation and rate-controlled input such as the RWP, the basic model-free ADRC formulation may not achieve satisfactory performance, as it does not explicitly accommodate the input differentiation, nor exploit available model information. This motivates the modified ADRC schemes presented in the following subsections.

3.2. ADRC approach with the system order reduction

The first structure proposition involves incorporating information about the coefficients and nature of the model into the synthesis of the control system, allowing for improved performance compared to the basic ADRC algorithm, presented in the previous subsection. In further considerations, it is assumed that the parameter $\hat{b}_0 = b_0$ is perfectly known.

After linearization of (3) at the operating point $\varphi = \varphi_0$ and assuming the presence of a disturbance function, the equation of motion for the synthesis of the ADRC controller is obtained:

$$\begin{aligned}\varphi^{(3)} = &-a_0 c_1 \gamma_J \cos(\varphi_0)\varphi - (a_0 \cos(\varphi_0) + a_1 c_1 \gamma_J)\dot{\varphi} + \\ &- (a_1 + c_1 \gamma_J)\ddot{\varphi} - b_0 \dot{u} + \dot{f}(\cdot),\end{aligned} \tag{17}$$

where the structure reflects that the control action influences the system through its time derivative. The total disturbance function represents modeling and linearization errors:

$$\begin{aligned}\dot{f}(\cdot) = &\, g(\cdot) + d + a_0 c_1 \gamma_J (\cos(\varphi_0)\varphi - \sin(\varphi)) + \\ &+ a_0(\cos(\varphi_0) - \cos(\varphi))\dot{\varphi},\end{aligned} \tag{18}$$

where d is the external disturbance signal, and g means the unmodeled system part.

In order to compensate for the derivative nature of the excitation (in order to match the ADRC structure), a two-sided integration of equation (17) was proposed:

$$\begin{aligned}\ddot{\varphi} = &-(a_0 \cos(\varphi_0) + a_1 c_1 \gamma_J)\varphi - (a_1 + c_1 \gamma_J)\dot{\varphi} + \\ &\underbrace{- b_0 u - a_0 c_1 \gamma_J \cos(\varphi_0) \int_0^t \varphi \, \mathrm{d}t + f(\cdot)}_{f_r(\cdot)},\end{aligned} \tag{19}$$

where the disturbance function f_r for the reduced system additionally contains information about the integral of the output.

State-space equations for the reduced model, in which $\underline{x}_r = \begin{bmatrix} \varphi & \dot{\varphi} & f_r \end{bmatrix}^{\top}$, can be described as

$$\begin{cases} \dot{\underline{x}}_r = \mathbf{A}_r \underline{x}_r - \underline{b}_r b_0 u + \underline{h}_r \dot{f}, \\ y = \underline{c}_r^{\top} \underline{x}_r, \end{cases} \tag{20}$$

where

$$\begin{aligned}\mathbf{A}_r &= \begin{bmatrix} 0 & 1 & 0 \\ -(a_0 \cos(\varphi_0) + a_1 c_1 \gamma_J) & -(a_1 + c_1 \gamma_J) & 1 \\ -a_0 c_1 \gamma_J \cos(\varphi_0) & 0 & 0 \end{bmatrix}, \\ \underline{b}_r &= \begin{bmatrix} 0 \\ 1 \\ 0 \end{bmatrix}, \quad \underline{h}_r = \begin{bmatrix} 0 \\ 0 \\ 1 \end{bmatrix}, \quad \underline{c}_r^{\top} = \begin{bmatrix} 1 & 0 & 0 \end{bmatrix}.\end{aligned} \tag{21}$$

The reduced-order model matrices are indicated by the subscript r.

Remark 2. Note that, because of the presence of the integral part in the total disturbance function f_r, there is a need to include this information in the system matrix. Otherwise, the presence of an uncompensated integral term in the disturbance function would result in a steady-state error in the system.

Since the scaling coefficient of the integral is known as prior, this information can be incorporated into the disturbance function equation, which simplifies the estimation of the disturbance function f_r and ensures a zero steady-state value of the system response:

$$\dot{f}_r = -a_0 c_1 \gamma_J \cos(\varphi_0)\varphi + \dot{f}. \tag{22}$$

Extended state observer

For the considered system structure, the ESO is given as follows:

$$\begin{cases} \dot{\hat{\underline{x}}}_r = (\mathbf{A}_r - \underline{l}\underline{c}_r^{\top})\hat{\underline{x}}_r - \underline{b}_r \hat{b}_0 u + \underline{l} y, \\ \hat{y} = \underline{c}_r^{\top} \hat{\underline{x}}_r, \end{cases} \tag{23}$$

where $l = \begin{bmatrix} l_1 & l_2 & l_3 \end{bmatrix}^{\top}$ is the ESO gains vector.

Controller

The outer control loop reduces the model equation to the form with a new input signal [37]:

$$\ddot{\varphi} = -\left(a_0\cos(\varphi_0) + a_1 c_1 \gamma_J\right)\varphi - \left(a_1 + c_1\gamma_J\right)\dot{\varphi} + u_0\,, \tag{24}$$

where the control law is given by equation

$$u_0 = k_1 y_r - \underline{k}^{\mathrm{T}}\underline{\hat{x}}_r\,. \tag{25}$$

The final control signal is obtained as follows

$$u = \frac{1}{\hat{b}_0}\left(u_0 - \hat{f}_r\right). \tag{26}$$

In order to obtain the state feedback gains, the pole placement method has also been used.

3.3. ADRC approach for two output signals

In this approach, two equations describing the system are separated, and a separate disturbance function is introduced for each of them:

$$\begin{cases} \ddot{\varphi} = -a_0\cos(\varphi_0)\varphi - a_1\dot{\varphi} + c_1\omega - b_0 u & + f_1(\cdot), \\ \dot{\omega} = \qquad -\gamma_J\left(c_1\omega - b_0 u\right) & + f_2(\cdot), \end{cases} \tag{27}$$

where f_1 and f_2 are the total disturbance functions in the pendulum arm and the DC motor path, respectively. Two output signals are considered, both affected by the same control input. The control system is therefore underactuated.

Assuming the state vector $\underline{x} = \begin{bmatrix}\varphi & \dot{\varphi} & \omega & f_1 & f_2\end{bmatrix}^{\top}$ and output vector $\underline{y} = \begin{bmatrix}\varphi & \omega\end{bmatrix}^{\top}$, state-space model of (27) is given as follows

$$\begin{cases} \dot{\underline{x}} = \mathbf{A}\underline{\hat{x}} + \mathbf{B}\underline{b}b_0 u + \mathbf{H}\underline{\dot{f}}, \\ \underline{y} = \mathbf{C}\underline{x}, \end{cases} \tag{28}$$

where matrices describing the plant are

$$\mathbf{A} = \begin{bmatrix} 0 & 1 & 0 & 0 & 0 \\ -a_0\cos(\varphi_0) & -a_1 & c_1 & 1 & 0 \\ 0 & 0 & 0 & -\gamma_J c_1 & 1 \\ 0 & 0 & 0 & 0 & 0 \\ 0 & 0 & 0 & 0 & 0 \end{bmatrix},$$

$$\mathbf{B} = \begin{bmatrix} -1 & 0 & 0 & 0 & 0 \\ 0 & -1 & 0 & 0 & 0 \\ 0 & 0 & \gamma_J & 0 & 0 \\ 0 & 0 & 0 & 0 & 0 \\ 0 & 0 & 0 & 0 & 0 \end{bmatrix}, \quad \underline{b} = \begin{bmatrix} 0 \\ 1 \\ 1 \\ 0 \\ 0 \end{bmatrix}, \quad \mathbf{H} = \begin{bmatrix} 0 & 0 \\ 0 & 0 \\ 0 & 0 \\ 1 & 0 \\ 0 & 1 \end{bmatrix}, \tag{29}$$

$$\mathbf{C} = \begin{bmatrix} \underline{c}_1^{\top} \\ \underline{c}_2^{\top} \end{bmatrix} = \begin{bmatrix} 1 & 0 & 0 & 0 & 0 \\ 0 & 0 & 1 & 0 & 0 \end{bmatrix}, \quad \underline{\dot{f}} = \begin{bmatrix} \dot{f}_1 \\ \dot{f}_2 \end{bmatrix}.$$

Extended state observer

In this case, the extended state observer is given by the set of equations:

$$\begin{cases} \dot{\underline{\hat{x}}} = (\mathbf{A} - \mathbf{L}\mathbf{C})\underline{\hat{x}} + \mathbf{B}\underline{b}\hat{b}_0 u + \mathbf{L}\underline{y}, \\ \underline{\hat{y}} = \mathbf{C}\underline{\hat{x}}, \end{cases} \tag{30}$$

where the observer gain matrix $\mathbf{L}$ consists of two vectors corresponding to the estimation error of the pendulum arm angular position and the reaction wheel angular velocity, respectively:

$$\mathbf{L} = \begin{bmatrix} \underline{l}_1 & \underline{l}_2 \end{bmatrix} \in \mathbb{R}^{5\times 2}. \tag{31}$$

Controller

For the purpose of designing the control algorithm, new control signals should be introduced to decouple the linear part of the internal dynamics. The system of equations is then transformed into the form

$$\begin{cases} \ddot{\varphi} = -a_0\cos(\varphi_0)\varphi - a_1\dot{\varphi} + c_1\omega & + u_{0,\varphi}, \\ \dot{\omega} = -\gamma_J c_1\omega & + u_{0,\theta}\,. \end{cases} \tag{32}$$

With a single control signal available in the control system, a state feedback and a decoupling loop are constructed in order to simultaneously influence both considered measurement signals. The control law for the inner decoupling loop is derived based on the state feedback, taking into account the coefficients from the matrix $\mathbf{B}$ corresponding to the individual dynamic equations of system (27). The control law in the inner loop is

$$\begin{aligned} u_0 &= -\begin{bmatrix} k_1 & k_2 & k_3 \end{bmatrix}\begin{bmatrix} -1 & 0 & 0 \\ 0 & -1 & 0 \\ 0 & 0 & \gamma_J^{-1} \end{bmatrix}\begin{bmatrix} \hat{x}_1 \\ \hat{x}_2 \\ \hat{x}_3 \end{bmatrix} = \\ &= \underbrace{-\left(-\begin{bmatrix} k_1 & k_2 \end{bmatrix}\begin{bmatrix} \hat{x}_1 \\ \hat{x}_2 \end{bmatrix}\right)}_{u_{0,\varphi}} + \gamma_J^{-1}\underbrace{\left(-k_3\hat{x}_3\right)}_{u_{0,\theta}}. \end{aligned} \tag{33}$$

And the final control signal for the system is

$$u = \frac{1}{\hat{b}_0}\left(u_0 - \begin{bmatrix} -1 & \gamma_J^{-1} \end{bmatrix}\begin{bmatrix} \hat{f}_1(\cdot) \\ \hat{f}_2(\cdot) \end{bmatrix}\right) = \frac{1}{\hat{b}_0}\left(u_0 + \hat{x}_4 - \gamma_J^{-1}\hat{x}_5\right). \tag{34}$$

Remark 3. For an approach with two disturbance functions in an underactuated system, it is not possible to achieve full compensation for the disturbance of the system by the control signal in every degree of freedom. As a result of the system operation, residual errors will occur, as illustrated below:

$$\begin{cases} \ddot{\varphi} = f_{l,1}(\cdot) + u_{0,\varphi} \underbrace{- \dfrac{1}{\gamma_J}\left(u_{0,\theta} - \hat{x}_5\right) + \left(f_1(\cdot) - \hat{x}_4\right)}_{\text{residual errors}}, \\ \dot{\omega} = f_{l,2}(\cdot) + u_{0,\theta} \underbrace{-\gamma_J\left(u_{0,\varphi} - \hat{x}_4\right) + \left(f_2(\cdot) - \hat{x}_5\right)}_{\text{residual errors}}, \end{cases}$$

where the linear model parts are given as follows:

$$f_{l,1}(\cdot) = -a_0 \cos(\varphi_0)\varphi - a_1\dot{\varphi} + c_1\omega,$$
$$f_{l,2}(\cdot) = -\gamma_J c_1 \omega.$$

The problem of global stabilization of an inverted pendulum on a cart (which represents an analogous problem to the one considered in the present work) was analyzed in [22] using Lyapunov analysis.

LQR approach for the considered control system

For a real RWP-type system with two outputs, selecting controller gains using the pole placement method would be practically difficult, especially when assigning a single multiple pole for the entire closed-loop system [38]. Choosing an appropriate pole distribution (with distinct or complex poles) is generally challenging and not intuitive. Therefore, the state feedback gains in (33) were determined using the linear quadratic regulator (LQR) approach, minimizing the performance index

$$J = \int_0^\infty \left(\underline{x}_n^{\mathrm{T}} \mathbf{Q}_c \underline{x}_n + q_u u^2\right) \mathrm{d}t, \tag{35}$$

where $\mathbf{Q}_c \in \mathbb{R}^{n\times n}$ is a diagonal cost matrix for the state vector components $\underline{x}_n = [\varphi\ \dot{\varphi}\ \omega]^\top$, and $q_u \in \mathbb{R}_+$ is the control input weight. Further analysis was carried out for the adopted RWP system order $n = 3$.

The state feedback gain vector $\underline{k}^\top = \begin{bmatrix} k_1 & k_2 & k_3 \end{bmatrix}$ is calculated as

$$\underline{k}^\top = \frac{1}{q_u} \underline{b}_n{}^\top \mathbf{P}_c, \tag{36}$$

where the covariance matrix $\mathbf{P}_c$ is obtained by solving the algebraic Riccati equation

$$\mathbf{A}_n^\top \mathbf{P}_c + \mathbf{P}_c \mathbf{A}_n - \frac{1}{q_u} \mathbf{P}_c \underline{b}_n \underline{b}_n^\top \mathbf{P}_c + \mathbf{Q}_c = \mathbf{0}. \tag{37}$$

The weighting matrix for the state variables in the control law is given by

$$\mathbf{Q}_c = \mathrm{diag}\{q_\varphi, q_{\dot{\varphi}}, q_\omega\}. \tag{38}$$

Note that the stability analysis for the considered ADRC methods is included in Appendix A.

Practical considerations

In the real RWP setup the reaction wheel actuator is voltage-limited, which implies speed limitations and possible input saturation. These constraints are naturally reflected in the swing-up-and-balance experiments, where the control signal $u(t)$ reaches its admissible bounds (see experimental results below). In the two-output ADRC formulation the LQR weights (Q_c, q_u) allow one to trade off pendulum stabilization performance against excessive wheel acceleration, thus mitigating the adverse effect of saturation. In practice, increasing the weight on the wheel velocity component suppresses the wheel speed and prevents runaway behavior without the need for additional anti-windup or rate limiting mechanisms.

Furthermore, the implementation of the ADRC control system includes a kind of anti-windup compensator due to the information about the control signal sample being fed to the ESO after passing through the Saturation block.

4. EXPERIMENTAL RESULTS

Experiments of the *swing-up-down* type were carried out with the stabilization of the pendulum position alternately in the upper position for $y_r = \pi$ and the lower position for $y_r = 0$, switching every 20 s:

$$y_r(t) = \frac{\pi}{2}\mathrm{sgn}\left(\sin\left(2\pi\frac{1}{40}t\right)\right) + \frac{\pi}{2}\ \ [\mathrm{rad}].$$

The classical model-free ADRC was compared with the proposed ADRC approaches. Experimental results can be found in Figs. 3–6. The normalized lower and upper positions are denoted φ_{down} and φ_{up}, respectively.

Remark 4. For stabilization at the upper equilibrium point, an energy-based control algorithm was implemented in hardware, designed to swing up the pendulum to the region where $|y - y_r| < 0.3$ rad [25]. When this condition is satisfied, the control algorithm switches, and the ADRC takes over. The energy-based control, however, is not the subject of this study.

For the basic ADRC approach, without including the information about the model into the control system synthesis (Fig. 3), overshoot occurs at both positions, and the response exhibits oscillations at the lower position. At the upper equilibrium, accumulation of the entire model dynamics in the total disturbance function leads to a steady-state error. The reaction wheel accelerates increasingly to compensate, causing system destabilization, noticeable at the end of each first half-period of the reference signal. At the lower position, the pendulum angle reaches the setpoint, but neglecting model parameters in the state vector introduces oscillatory modes in the closed-loop system. Due to dynamic differences at the two operating points, achieving the same regulation quality requires retuning ESO gains and state feedback.

For the reduced-order control in the algorithm (Fig. 4), the impact of disturbance is reduced, eliminating oscillations due to the differentiating nature of the plant. Stabilization at both operating points occurs without overshoot. Maintaining the differentiating behavior in the state-space model allows using the nominal input scaling from the plant equations, unlike previous ADRC variants. Neglecting flywheel speed can still cause destabilization at the upper position, while small calibration errors may introduce integrator-like accumulation in the disturbance function (19).

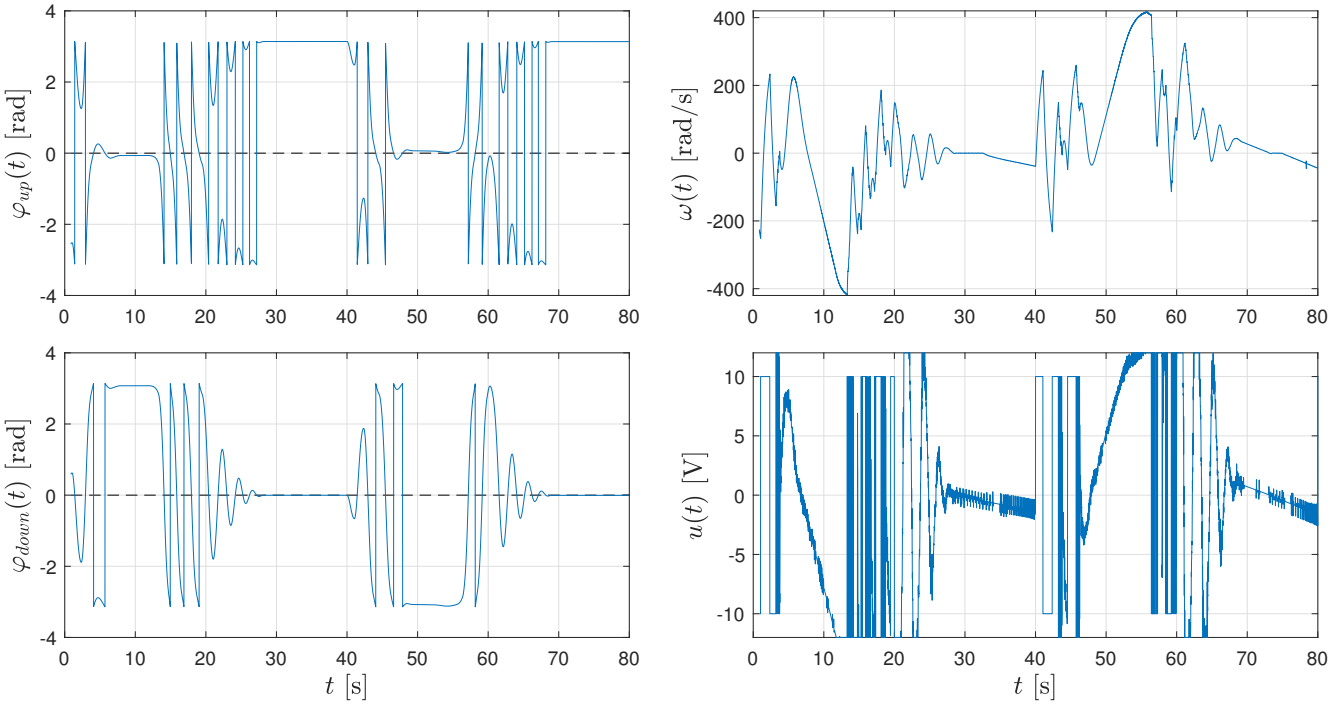

Fig. 3. Experimental results for the basic ADRC approach with parameters: $\hat{b}_0 = 8$, $\omega_c = 4$, $\omega_o = 30$

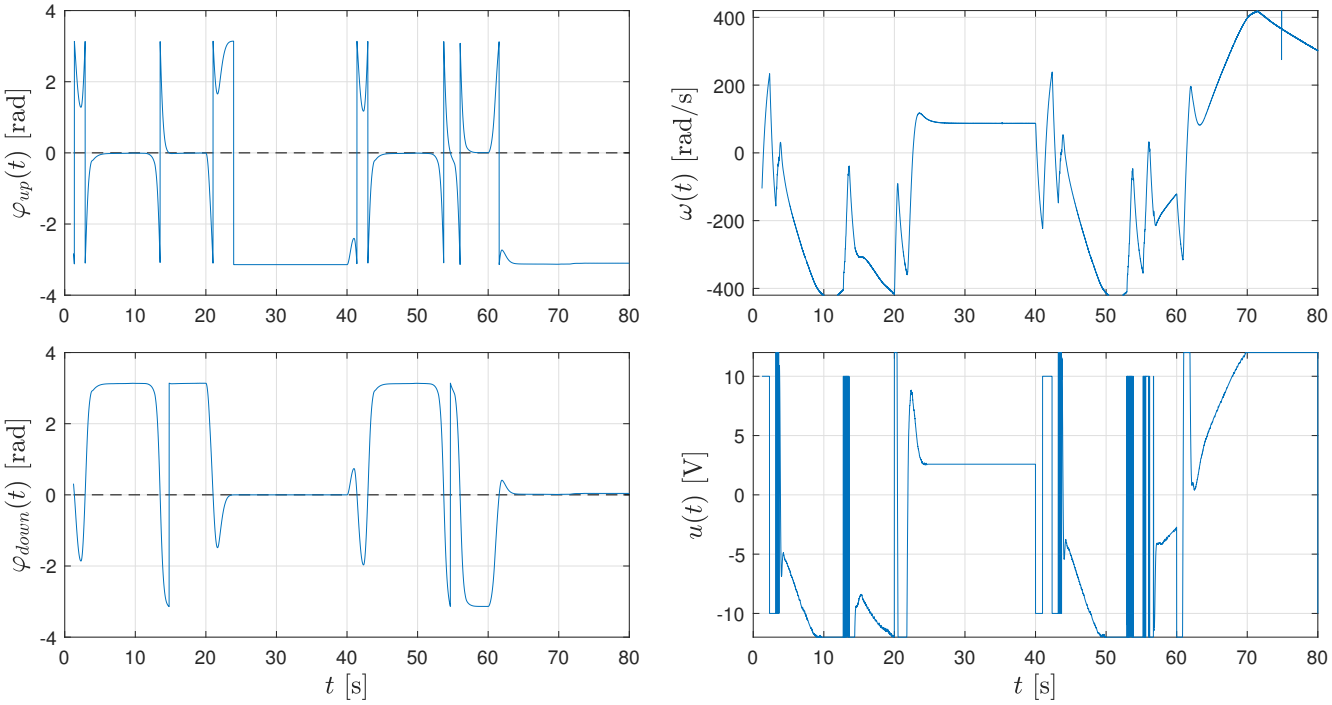

Fig. 4. Experimental results of the reduced-order ADRC approach, for parameters: $\hat{b}_0 = b_0 = 0.3388$, $\omega_c = 3$, $\omega_o = 15$

The results for the control of two output signals with nominal settings are shown in Figs. 5 and 6. LQR tuning was used for state feedback, balancing the weights between pendulum stabilization and flywheel speed limitation. With nominal settings, the system is stable at both points, the pendulum maintains its desired position, and the flywheel velocity is constrained. Some overshoot may occur due to incomplete disturbance compensation between the two outputs.

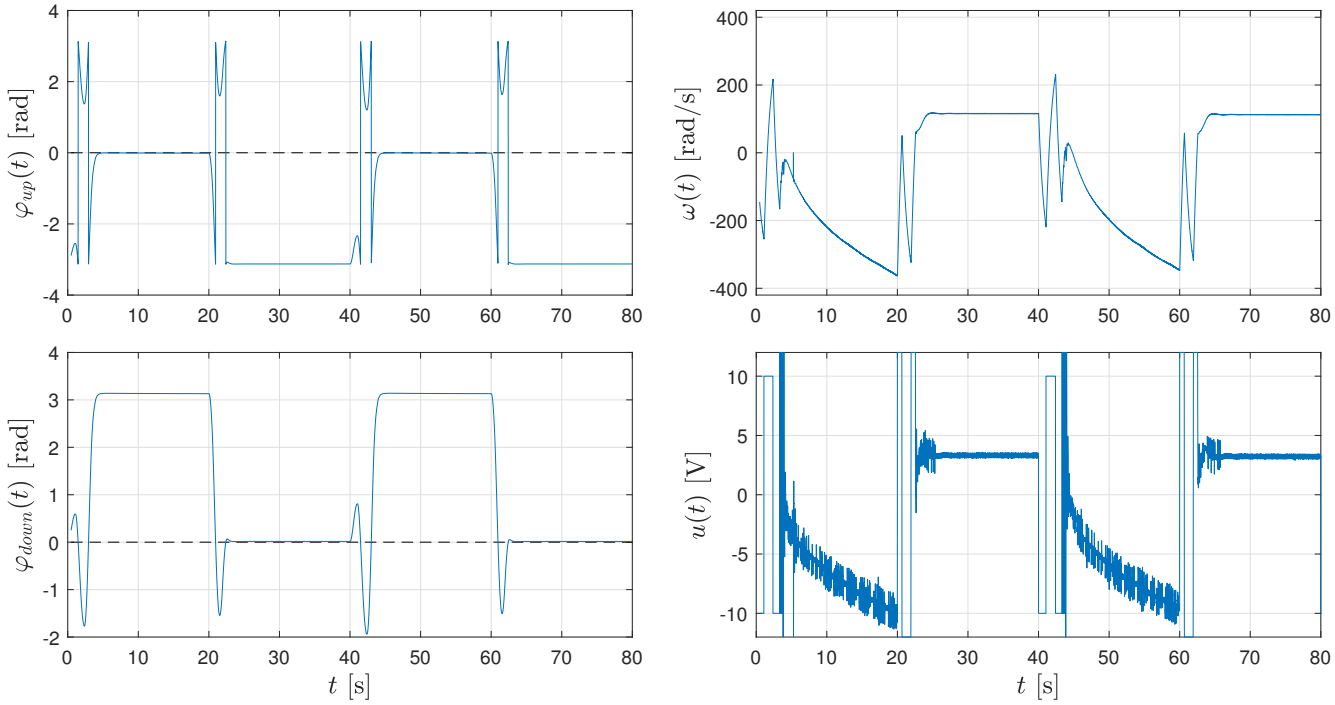

Fig. 5. Experimental results for LQR approach (2 outputs) with parameters: $\hat{b}_0 = b_0 = 0.3388$, $\mathbf{Q}_c = \text{diag}\{100000, 8000, 200\}$, $q_u = 15$, $\omega_o = 30$

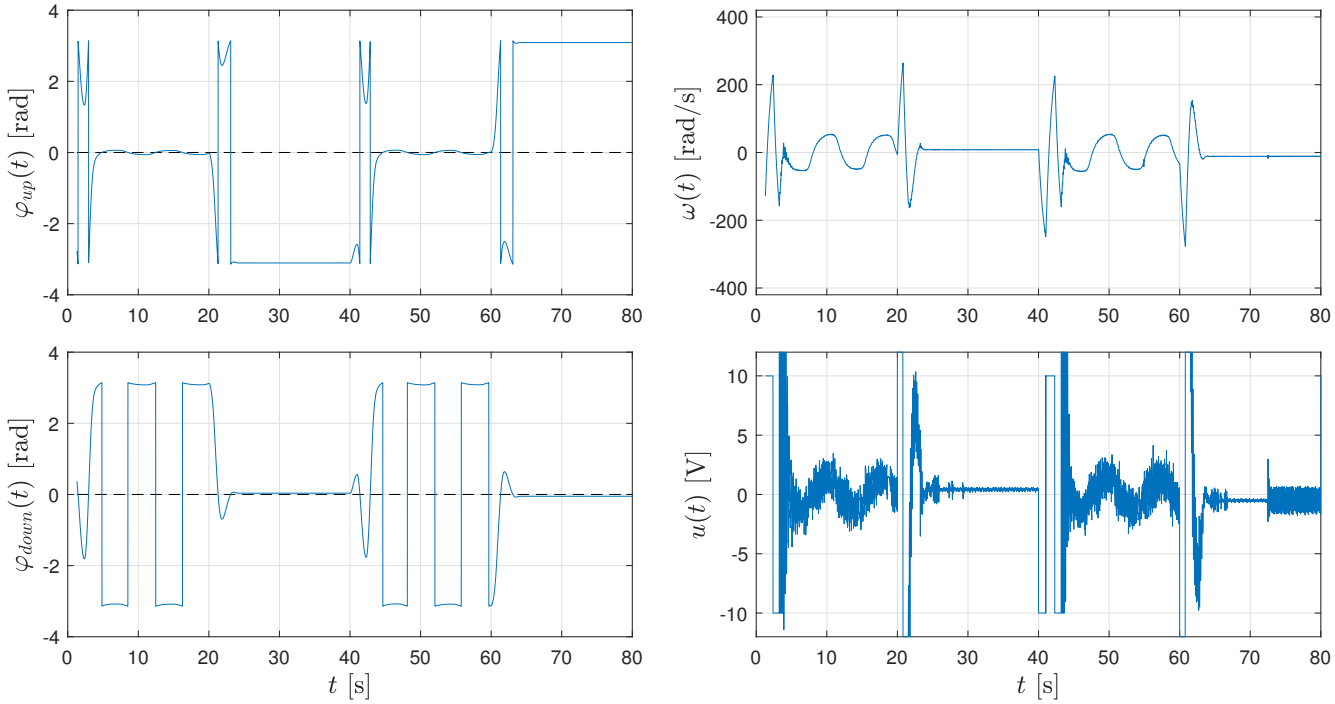

Fig. 6. Experimental results for LQR approach (2 outputs) with parameters: $\hat{b}_0 = b_0 = 0.3388$, $\mathbf{Q}_c = \text{diag}\{100000, 8000, 40000\}$, $q_u = 15$, $\omega_o = 30$

Adjusting the state weight matrix (increasing the third state weight) achieves a compromise between pendulum stabilization and zeroing flywheel speed. The nominal weights were set as

$$\mathbf{Q}_c = \text{diag}\{100000, 8000, 200\},\ q_u = 15,$$

with the placement of the observer pole at the bandwidth value $\omega_o = 30$. The technical information about the theoretical aspects and experimental/practical results are summarized in Table 1.

Table 1
Comparison of ADRC variants evaluated for the reaction–wheel pendulum

Feature	Baseline ADRC	Reduced-order ADRC	Two-output ADRC (LQR)
Input structure	Assumes affine input; differentiating input ($\dot{u}$) violates the standard ADRC model.	Differentiating input analytically compensated by double integration; restores affine input form.	Single input shared by two outputs; inner decoupling loop shapes the effective input for both channels.
Model knowledge used	No explicit model; fully model-free tuning.	Linearized coefficients and known integral term included in the reduced model.	Linearized two-path model (pendulum and wheel) and structure exploited in LQR feedback.
Disturbance representation	Total disturbance accumulates full dynamics; risk of steady-state drift and oscillations.	Known integral contribution extracted from disturbance, preventing bias in steady state.	Two disturbance channels; only partial disturbance compensation possible due to underactuation.
Experimental behavior	Overshoot and oscillations; degradation at the upper equilibrium due to accumulation in the ESO.	No overshoot; stable regulation at both upper and lower positions; improved robustness to model nonlinearities.	Stable at both positions; clear trade-off between pendulum regulation and wheel velocity suppression.
Tuning aspects	Tuning difficult because the real input path is not affine; gains must be found empirically.	Nominal gain b_0 from the plant model can be used; tuning follows standard ADRC rules.	Requires selection of LQR weights (Q_c, q_u) to balance performance of both outputs.
Typical use-case	Plants close to the ideal ADRC structure with well-behaved input channel.	Systems with differentiating input and partly known parameters.	Underactuated systems with two measured outputs and shared actuation (reaction-wheel type).

5. CONCLUSIONS

This work investigated the problem of applying active disturbance rejection control to a reaction–wheel pendulum, a nonlinear underactuated system whose dynamics violate the standard assumptions of the classical ADRC formulation. The differentiating behavior of the input channel and the coupling between mechanical subsystems were shown to directly affect observer performance and the achievable regulation quality.

By incorporating selected structural information about the plant, two modified ADRC formulations were developed and experimentally validated. Both methods enabled stable operation at the upper and lower equilibrium positions and demonstrated that even limited model knowledge can substantially improve control performance in systems with non-affine input dynamics.

The results indicate that extending the ADRC framework beyond its purely model-free formulation is beneficial when dealing with underactuation or derivative-type input characteristics. These findings motivate further research toward nonlinear, adaptive, and gain-scheduled ADRC variants, as well as extensions that address stronger couplings or additional degrees of freedom in reaction-wheel-type systems.

APPENDIX A. STABILITY CONSIDERATIONS

Assumptions and notation

We address three cases discussed in the paper: (i) baseline ADRC in the integrator-chain form, (ii) the order-reduction approach that compensates the derivative in the input path, and (iii) the two-output version with the inner decoupling/LQR loop.

We adopt standard ADRC assumptions:

A1) The input gain b_0 is known and positive (where noted, the nominal b_0 is used).

A2) The total disturbance $f(\cdot)$ is continuous with bounded derivative: $\|\dot{f}(t)\| \le \bar{d}$.

A3) In the reduced-order variant, the known integral coefficient is explicitly accounted for (22), which removes a steady-state bias otherwise induced by the "naked" integral in f_r.

Define the observer error $\underline{\tilde{x}} := \underline{x} - \underline{\hat{x}}$ and the tracking error $e := y - y_r$.

A.1. Baseline ADRC

The system model is given by (7), and $\hat{b}_0 = b_0$. With ESO poles placed via $(s+\omega_o)^{n+1}$, the estimation error dynamics are

$$\dot{\underline{\tilde{x}}} = (\mathbf{A} - \underline{l}\underline{c}^{\top})\underline{\tilde{x}} + \underline{h}\,\dot{f}, \tag{39}$$

where $(\mathbf{A} - \underline{l}\underline{c}^{\top})$ is Hurwitz (all poles at $-\omega_o$). Standard linear-system estimates yield, for some $\lambda > 0$ and $C_o > 0$,

$$\|\underline{\tilde{x}}(t)\| \le C_o\, \mathrm{e}^{-\lambda\omega_o t}\|\underline{\tilde{x}}(0)\| + \frac{C_o}{\lambda\omega_o}\,\bar{d},$$

so that $\underline{\tilde{x}}$ can be made arbitrarily small by increasing ω_o.

The ADRC law (15) with state feedback (14) yields the closed-loop error channel

$$e^{(n)} + k_n e^{(n-1)} + \cdots + k_2\dot{e} + k_1 e = \underline{v}^{\top}\underline{\tilde{x}}, \qquad \underline{v} := \begin{bmatrix} \underline{k} \\ 1 \end{bmatrix}, \tag{40}$$

where $\underline{k}$ is the feedback gain from (14). Thus the error dynamics are a linear Hurwitz system driven by the input $\underline{v}^{\top}\underline{\tilde{x}}$, which is bounded by $|\underline{v}^{\top}\underline{\tilde{x}}| \le \|\underline{v}\|\,\|\underline{\tilde{x}}\|$.

Since $\underline{\tilde{x}}$ is ISS (input-to-state stable in the standard linear sense) for bounded $\dot{f}$, and (40) is linear in $\underline{\tilde{x}}$, the cascade implies ISS of the overall closed-loop system. In the ideal-ESO limit $\underline{\tilde{x}} \equiv 0$ (formally, $\omega_o \to \infty$ with bounded $\dot{f}$), (40) reduces to a homogeneous linear equation and $e(t) \to 0$ locally exponentially, with convergence rates set by ω_c (controller) and ω_o (ESO).

Result A.1 (Local stability of baseline ADRC). Under A1–A2 and with $\omega_o > 0$ and gains chosen so that $(\mathbf{A} - \underline{l}\underline{c}^\top)$ and the companion matrix associated with $\phi(s) = s^n + k_n s^{n-1} + \cdots + k_1$ are Hurwitz, the closed-loop system is locally ISS for $\dot{f}$ and locally asymptotically (in fact, exponentially) stable for $\dot{f} \equiv 0$.

It should be noted that in the examined case of the RWP system, an additional structural uncertainty appears in the disturbance function due to the derivative in the input path.

A.2. Order–reduction with derivative–input compensation

After performing the two–sided integration of (17), one obtains the reduced state $\underline{x}_r$ governed by (19) together with the modified disturbance evolution (22). The ESO (23) yields the estimation–error dynamics

$$\dot{\underline{\tilde{x}}}_r = (\mathbf{A}_r - \underline{l}\,\underline{c}_r^\top)\,\underline{\tilde{x}}_r + \underline{h}_r\,\dot{f},$$

where $\underline{\tilde{x}}_r$ collects the state and disturbance errors in the reduced model.

Recall that the reduced-order model (19) introduces the coefficients $\alpha_1 > 0$ and $\alpha_0 > 0$ in

$$\ddot{\varphi} + \alpha_1\dot{\varphi} + \alpha_0\varphi = f_r + b_0 u,$$

which lead to the tracking-error dynamics

$$\ddot{e} + \alpha_1\dot{e} + \alpha_0 e = \underline{k}^\top\underline{\tilde{x}}_r + \tilde{f}_r.$$

Using the controller (24)–(26) and defining $\underline{z} := [\,e,\ \dot{e}\,]^\top$, the tracking error evolves as

$$\dot{\underline{z}} = \mathbf{A}_c\,\underline{z} + \underline{b}_c\,\big(\underline{k}^\top\underline{\tilde{x}}_r + \tilde{f}_r\big), \tag{41}$$

where $\mathbf{A}_c = \begin{bmatrix} 0 & 1 \\ -\alpha_0 & -\alpha_1 \end{bmatrix}$, $\underline{b}_c = \begin{bmatrix} 0 \\ 1 \end{bmatrix}$ follows from the nominal reduced–order dynamics and is Hurwitz for all $\alpha_0 > 0$ and $\alpha_1 > 0$ for the selected gains (25).

Consider the quadratic Lyapunov function

$$V(\underline{z}) = \underline{z}^\top\mathbf{P}\,\underline{z}, \qquad \mathbf{A}_c^\top\mathbf{P} + \mathbf{P}\mathbf{A}_c = -\mathbf{Q},$$

with $\mathbf{P} = \mathbf{P}^\top > 0$, $\mathbf{Q} = \mathbf{Q}^\top > 0$. Differentiating V along the trajectories of (41) gives

$$\dot{V} = -\underline{z}^\top\mathbf{Q}\,\underline{z} + 2\,\underline{z}^\top\mathbf{P}\,\underline{b}_c\,\big(\underline{k}^\top\underline{\tilde{x}}_r + \tilde{f}_r\big).$$

Using the Cauchy–Schwarz inequality and $\underline{z}^\top\mathbf{Q}\,\underline{z} \geq \lambda_{\min}(\mathbf{Q})\|\underline{z}\|^2$ yields

$$\dot{V} \leq -\lambda_{\min}(\mathbf{Q})\,\|\underline{z}\|^2 + 2\,\|\mathbf{P}\underline{b}_c\|\,\|\underline{z}\|\,\big(\|\underline{k}\|\,\|\underline{\tilde{x}}_r\| + |\tilde{f}_r|\big),$$

which shows ISS of $\underline{z}$ with respect to $\underline{\tilde{x}}_r$ and $\tilde{f}_r$. For $\dot{f} \equiv 0$ (and hence $\underline{\tilde{x}}_r \to 0$, $\tilde{f}_r \to 0$) the linear part dominates and the closed loop is locally exponentially stable.

Result A.2 (Local stability for the reduced-order variant). Under A1–A3, with $(\mathbf{A}_r - \underline{l}\underline{c}_r^\top)$ and $\mathbf{A}_c$ Hurwitz for the chosen gains, the reduced-order control system is locally ISS for bounded $\dot{f}$ and locally exponentially stable for $\dot{f} \equiv 0$.

A.3. Two-output system with LQR

For the system (27), we use local linearization around the operating point (32), the inner feedback/decoupling loop, and LQR on $\underline{x}_n = \begin{bmatrix} \varphi & \dot{\varphi} & \omega \end{bmatrix}^\top$. The ESO is matrix-valued (30) with gains vector (31); the estimation error satisfies

$$\dot{\underline{\tilde{x}}} = (\mathbf{A} - \mathbf{L}\mathbf{C})\underline{\tilde{x}} + \mathbf{H}\,\dot{\underline{f}},$$

and, for bounded $\dot{\underline{f}}$, remains bounded with a standard ISS-type estimate.

The final control law

$$u = \frac{1}{b_0}\Big(u_0 + \hat{f}_1 - \gamma_J^{-1}\hat{f}_2\Big), \tag{42}$$

implies (Remark 3) residual couplings that depend on estimation errors and the transformed disturbances.

Let $\mathbf{P}_c = \mathbf{P}_c^\top > 0$ solve the algebraic Riccati equation (ARE) for $(\mathbf{A}_n, \underline{b}_n)$ with weights $(\mathbf{Q}_c, q_u)$ from Section 3.3; then the choice of $\underline{k}^\top$ makes $(\mathbf{A}_n - \underline{b}_n\underline{k}^\top)$ Hurwitz. Consider

$$V(\underline{x}_n, \underline{\tilde{x}}) = \underline{x}_n^\top\mathbf{P}_c\underline{x}_n + \underline{\tilde{x}}^\top\mathbf{S}\underline{\tilde{x}},$$

where $\mathbf{S} = \mathbf{S}^\top > 0$ solves a Lyapunov equation for $(\mathbf{A} - \mathbf{L}\mathbf{C})$. In closed loop (with (42)) one obtains a bound of the form

$$\dot{V} \leq -\underline{x}_n^\top\mathbf{Q}_c\underline{x}_n - \underline{\tilde{x}}^\top\mathbf{Q}_o\underline{\tilde{x}} + c_1\|\underline{x}_n\|\,\|\underline{\tilde{x}}\| + c_2\|\underline{x}_n\|\,\|\dot{\underline{f}}\|,$$

for some $c_1, c_2 > 0$ and $\mathbf{Q}_o = \mathbf{Q}_o^\top > 0$. For sufficiently small $\|\dot{\underline{f}}\|$ and in a local region where nonlinear residuals are small, this yields decay of V and thus local boundedness and convergence of $(\underline{x}_n, \underline{\tilde{x}})$.

In particular, for $\dot{\underline{f}} \equiv 0$ (and small enough nonlinear residuals, i.e., in a neighborhood of the operating point) the cross terms are dominated by the quadratic terms and the linearized closed loop is locally exponentially stable.

Result A.3 (ISS and local stability for the two-output system). Assume controllability of $(\mathbf{A}_n, \underline{b}_n)$ and observability of $(\mathbf{A}, \mathbf{C})$ in the linearization around the operating point, and A1–A3. Then the system (27) with the two-output ADRC structure is locally ISS with respect to $\dot{\underline{f}}$ and locally exponentially stable for $\dot{\underline{f}} \equiv 0$ (in a sufficiently small neighborhood of the equilibrium, due to underactuation and nonlinear couplings).

A.4. Final remarks and methods comparison

All three analyses follow the classical ADRC cascade argument: the ESO error acts as a small matched perturbation, while the nominal closed-loop dynamics are exponentially stable. Standard Lyapunov bounds therefore ensure ISS for bounded $\dot{f}$ and local exponential stability in the ideal estimation case.

The reduced-order ADRC yields nominal decoupled, linear error dynamics, which admit a single quadratic Lyapunov function and a perturbation term depending only on $\|\underline{\tilde{x}}_r\|$. This gives the cleanest exponential convergence for $\dot{f} \equiv 0$ and the smallest residual bound otherwise.

The two-output LQR structure couples plant and observer energies in a composite Lyapunov function. This ensures robustness and ISS with respect to $\dot{f}$, but exponential convergence holds only under sufficiently accurate estimation due to the coupling terms.

The baseline ADRC forms a cascade in which the tracking error depends directly on the ESO error; hence, only an ISS-type bound is available in general. In the ideal-ESO limit, however, the dynamics reduce to a homogeneous Hurwitz system and are locally exponentially stable.

Key practical observations:

(i) A larger ω_o speeds up ESO convergence but amplifies noise.

(ii) In the reduced-order scheme, including the known scaling (22) avoids steady-state bias.

(iii) In the two-output case, the weights $\mathbf{Q}_c = \mathrm{diag}\{q_\varphi, q_{\dot{\varphi}}, q_\omega\}$ and q_u determine the trade-off between ω suppression and φ regulation.

ACKNOWLEDGEMENTS

This work was financially supported by 0214/SBAD/0251.

REFERENCES

[1] J. Han, "From PID to active disturbance rejection control," *IEEE Trans. Ind. Electron.*, vol. 56, no. 3, pp. 900–906, 2009, doi: 10.1109/TIE.2008.2011621.

[2] Z. Gao, "Active disturbance rejection control: a paradigm shift in feedback control system design," in *2006 American Control Conference*. IEEE, 2006, pp. 2399–2405, doi: 10.1109/acc.2006.1656579.

[3] Y. Huang and W. Xue, "Active disturbance rejection control: Methodology and theoretical analysis," *ISA Trans.*, vol. 53, no. 4, pp. 963–976, 2014, doi: 10.1016/j.isatra.2014.03.003.

[4] G. Herbst, "A simulative study on active disturbance rejection control (ADRC) as a control tool for practitioners," *Electronics*, vol. 2, no. 3, pp. 246–279, 2013, doi: 10.3390/electronics2030246.

[5] G. Herbst, "Transfer function analysis and implementation of active disturbance rejection control," *Control Theory Technol.*, vol. 19, pp. 19–34, 2021, doi: 10.1007/s11768-021-00031-5.

[6] G. Herbst and R. Madonski, "Tuning and implementation variants of discrete-time ADRC," *Control Theory Technol.*, vol. 21, no. 1, pp. 72–88, 2023, doi: 10.1007/s11768-023-00127-0.

[7] R. Madonski, G. Herbst, and M. Stankovic, "ADRC in output and error form: Connection, equivalence, performance," *Control Theory Technol.*, vol. 21, no. 1, pp. 56–71, 2023, doi: 10.1007/s11768-023-00129-y.

[8] Z. Gao, "Scaling and bandwidth-parameterization based controller tuning," in *Active disturbance rejection control: a paradigm shift in feedback control system design*, 2003, pp. 4989–4996, doi: 10.1109/ACC.2003.1242516.

[9] Y.V. Hote and S. Jain, "Generalized active disturbance rejection control: Review, applications and challenges," in *2021 IEEE International Conference on Automation/XXIV Congress of the Chilean Association of Automatic Control (ICA-ACCA)*. IEEE, 2021, pp. 1–6.

[10] K. Łakomy, W. Giernacki, J. Michalski, and R. Madonski, "Active disturbance rejection control (ADRC) toolbox for MATLAB/Simulink," arXiv preprint arXiv:2112.01614, 2021, doi: 10.48550/arXiv.2112.01614.

[11] P. Kicki, K. Łakomy, and K.M.B. Lee, "Tuning of extended state observer with neural network-based control performance assessment," *Eur. J. Control*, vol. 64, p. 100609, 2022, doi: 10.1016/j.ejcon.2021.12.004.

[12] K. Łakomy and R. Madonski, "Cascade extended state observer for active disturbance rejection control applications under measurement noise," *ISA Trans.*, vol. 109, pp. 1–10, 2021, doi: 10.1016/j.isatra.2020.09.007.

[13] K. Łakomy, R. Madonski, B. Dai, J. Yang, P. Kicki, M. Ansari, and S. Li, "Active disturbance rejection control design with suppression of sensor noise effects in application to DC–DC buck power converter," *IEEE Trans. Ind. Electron.*, 2021, doi: 10.1109/TIE.2021.3055187.

[14] R. Madonski, M. Ramírez-Neria, M. Stankovic, S. Shao, Z. Gao, J. Yang, and S. Li, "On vibration suppression and trajectory tracking in largely uncertain torsional system: An error-based ADRC approach," *Mech. Syst. Signal Process.*, vol. 134, p. 106300, 2019, doi: 10.1016/j.ymssp.2019.106300.

[15] R. Madonski, M. Stankovic, S. Shao, Z. Gao, J. Yang, and S. Li, "Active disturbance rejection control of torsional plant with unknown frequency harmonic disturbance," *Control Eng. Pract.*, vol. 100, p. 104413, 2020, doi: 10.1016/j.conengprac.2020.104413.

[16] R. Patelski and D. Pazderski, "Tracking control for a cascade perturbed control system using the active disturbance rejection paradigm," *Arch. Control. Sci.*, vol. 29, no. 2, pp. 387–408, 2019, doi: 10.24425/acs.2019.129387.

[17] D. Pazderski, R. Patelski, B. Krysiak, and K. Kozłowski, "Analysis of an impact of inertia parameter in active disturbance rejection control structures," *Electronics*, vol. 9, no. 11, p. 1801, 2020, doi: 10.3390/electronics9111801.

[18] B. Wicher and S. Brock, "Tuning algorithm for ADRC speed control dedicated to two-mass system," *Przegląd Elektrotechniczny*, vol. 100, no. 5, pp. 49–55, 2024, doi: 10.15199/48.2024.05.09.

[19] Z.-g. Su, L. Sun, W. Xue, and K.Y. Lee, "A review on active disturbance rejection control of power generation systems: Fundamentals, tunings and practices," *Control Eng. Pract.*, vol. 141, p. 105716, 2023, doi: 10.1016/j.conengprac.2023.105716.

[20] R. Fareh, S. Khadraoui, M.Y. Abdallah, M. Baziyad, and M. Bettayeb, "Active disturbance rejection control for robotic systems: A review," *Mechatronics*, vol. 80, p. 102671, 2021, doi: 10.1016/j.mechatronics.2021.102671.

[21] M.W. Spong, P. Corke, and R. Lozano, "Nonlinear control of the reaction wheel pendulum," *Automatica*, vol. 37, no. 11, pp. 1845–1851, 2001, doi: 10.1016/S0005-1098(01)00145-5.

[22] B. Srinivasan, P. Huguenin, and D. Bonvin, "Global stabilization of an inverted pendulum–control strategy and experimental verification," *Automatica*, vol. 45, no. 1, pp. 265–269, 2009, doi: 10.1016/j.automatica.2008.07.004.

[23] M. Rosol, A. Pilat, and A. Tumau, "Time-optimal control for reaction wheel pendulum," in *Proc. 2016 21st International Conference on Methods and Models in Automation and Robotics (MMAR)*. IEEE, 2016, pp. 1057–1062, doi: 10.1109/MMAR.2016.7575284.

[24] Y. Sumioka, S. Sakaino, T. Satoh, and K. Ohnishi, "Motorcycle with reaction wheel pendulum: Swerving without steering around sharp bends," *IEEE Rob. Autom. Lett.*, vol. 8, no. 3, pp. 1580–1587, 2023, doi: 10.1109/LRA.2023.3241002.

[25] INTECO Sp. z o.o., "Reaction wheel pendulum." [Online]. Available: https://www.inteco.com.pl/products/reaction-wheel-pendulum

[26] J. Michalski, M. Mrotek, T. Tomczak, J. Wojciechowski, and D. Pazderski, "Reaction Wheel Pendulum Stabilization Using Various State-Space Representations," *Electronics*, vol. 14, no. 23, p. 4719, 2025, doi: 10.3390/electronics14234719.

[27] D.J. Block, K.J. Åström, and M.W. Spong, *The reaction wheel pendulum*. Morgan & Claypool Publishers, 2007, no. 1.

[28] O.D. Montoya and W. Gil-González, "Nonlinear analysis and control of a reaction wheel pendulum: Lyapunov-based approach," *Eng. Sci. Technol. Int. J.*, vol. 23, no. 1, pp. 21–29, 2020, doi: 10.1016/j.jestch.2019.03.004.

[29] O.D. Montoya, W. Gil-González, J.A. Dominguez-Jimenez, A. Molina-Cabrera, and D.A. Giral-Ramírez, "Global stabilization of a reaction wheel pendulum: a discrete-inverse optimal formulation approach via a control Lyapunov function," *Symmetry*, vol. 12, no. 11, p. 1771, 2020, doi: 10.3390/sym12111771.

[30] Y.E. Bezci *et al.*, "Classical and intelligent methods in model extraction and stabilization of a dual-axis reaction wheel pendulum: A comparative study," *Results Eng.*, vol. 16, p. 100685, 2022, doi: 10.1109/TMECH.2025.3572225.

[31] W.-H. Huang, P.T.-T. Nguyen, D.-D. Nguyen, H.-P. Doan, M.-Y. Chuang, and C.-H. Kuo, "Stability control and path tracking of a self-balancing bicycle with a reaction wheel," *IEEE/ASME Trans. Mechatron.*, 2025, doi: 10.1109/TMECH.2025.3572225.

[32] S.I. Abdelmaksoud, M.H.A. Al-Mola, and S.H. Mohamed, "Wheels in space: Modeling and comparative control analysis of a reaction wheel pendulum for space attitude stability," in *2025 International Telecommunications Conference (ITC-Egypt)*. IEEE, 2025, pp. 649–654, doi: 10.1109/ITC-Egypt66095. 2025.11186579.

[33] J. Michalski, M. Mrotek, and S. Brock, "Transfer function analysis and algorithm order reduction for active disturbance rejection control," in *Proc. 28th International Conference on Methods and Models in Automation and Robotics (MMAR)*. IEEE, 2024, pp. 591–596, doi: 10.1109/MMAR62187.2024.10680796.

[34] M. Mrotek and J. Michalski, "Trajectory tracking with generalized active disturbance rejection control using Kalman filter-based extended state observer," in *Proc.28th International Conference on Methods and Models in Automation and Robotics (MMAR)*. IEEE, 2024, pp. 316–321, doi: 10.1109/MMAR62187.2024.10680815.

[35] M. Mrotek, J. Michalski, R. Madonski, D. Pazderski, M. Retinger, and P. Kozierski, "Balancing Benefits and Risks of Embedding System Knowledge in Linear Active Disturbance Rejection Control," *Electronics*, vol. 14, no. 22, p. 4467, 2025.

[36] M. Mrotek, J. Michalski, E.W. Zurita-Bustamante, R. Madonski, and D. Pazderski, "Embedding System Knowledge in Nonlinear Active Disturbance Rejection Control: Insights from a Magnetic Levitation System," *Electronics*, vol. 14, no. 24, p. 4811, 2025, doi: 10.3390/electronics14244811.

[37] J. Michalski, M. Mrotek, M. Retinger, and P. Kozierski, "Adaptive active disturbance rejection control with recursive parameter identification," *Electronics*, vol. 13, no. 16, p. 3114, 2024, doi: 10.3390/electronics13163114.

[38] T. Sumioka, K. Akimoto, T. Tsujimura, S. Takayanagi, K. Fukushima, and T. Nose, "Rider cooperative control of rear-wheel-swing motorcycle based on divergent component of motion," *IEEE Rob. Autom. Lett.*, vol. 9, no. 1, pp. 223–230, 2023, doi: 10.1109/LRA.2023.3331658.